Density Functional Theory Study on the Structure and Capillary Phase Transition of a Polymer Melt in a Slitlike Pore: Effect of Attraction

Yang-Xin Yu,* Guang-Hua Gao, and Xiao-Lin Wang

Department of Chemical Engineering, Tsinghua University, Beijing 100084, People's Republic of China

Received: February 15, 2006; In Final Form: May 31, 2006

A density functional theory is proposed to investigate the effects of polymer monomer−monomer and monomer−wall attractions on the density profile, chain configuration, and equilibrium capillary phase transition of a freely jointed multi-Yukawa fluid confined in a slitlike pore. The excess Helmholtz energy functional is constructed by using the modified fundamental measure theory, Wertheim's first-order thermodynamic perturbation theory, and Rosenfeld's perturbative method, in which the bulk radial distribution function and direct correlation function of hard-core multi-Yukawa monomers are obtained from the first-order mean spherical approximation. Comparisons of density profiles and bond orientation correlation functions of inhomogeneous chain fluids predicted from the present theory with the simulation data show that the present theory is very accurate, superior to the previous theory. The present theory predicts that the polymer monomer−monomer attraction lowers the strength of oscillations for density profiles and bond orientation correlation functions and makes the excess adsorption more negative. It is interesting to find that the equilibrium capillary phase transition of the polymeric fluid in the hard slitlike pore occurs at a higher chemical potential than in bulk condition, but as the attraction of the pore wall is increased sufficiently, the chemical potential for equilibrium capillary phase transition becomes lower than that for bulk vapor−liquid equilibrium.

I. Introduction

Understanding the structure and thermodynamic properties of confined polymeric fluids is very important for many industrial applications such as surface coating, lubrication, and colloidal stability.[1] The interplay of the intermolecular interaction, chain connectivity, and the forces arising from solid surfaces makes the structure and phase behavior of confined polymeric fluids interesting but difficult to predict. In principle, molecular simulations,[2] polymer integral-equation approaches,[3] self-consistent-field theories,[4,5] and density functional theories (DFTs)[6] can be used to investigate the properties of polymeric fluids under inhomogeneous conditions. With explicit consideration of surface and intermolecular interactions, the density functional theories are very promising as a method for exploring the rich equilibrium phase behavior of confined polymeric fluid.

The key problem of a density functional theory is to develop an expression for the grand potential as a functional of density profiles.[7] There are two complementary ways to derive the grand potential: one is based on density expansion, and the other is based on weighted densities. The first way was initially introduced by Chandler, McCoy, and Singers (CMS).[8−10] Recently, more efficient methodologies have been proposed and successfully applied to the prediction of the structures, adsorptions, and surface tensions of freely jointed hard-sphere chain (HSC) fluids near hard surfaces.[11] The weighted-density approach for chain fluids was first proposed by Woodward[12] and by Kierlik and Rosinberg (KR).[13] Yethiraj and Woodward[14] presented a density functional theory that conbines an exact expression for the free energy of non-interacting chains, and Patra and Yethiraj[15] separated the Helmholtz free energy functional into a repulsive and an attractive contribution in which a Heaviside step function is used for the repulsive weighting function and a van der Waals approximation for the attractions. Unfortunately, the latter gives a rather poor representation of the equation of state. It should be noticeable that, in the implementation of a DFT for square-well chain fluids, Ye et al.[16,17] used a Heaviside step function for both repulsive and attractive weighting functions. In KR theory for chain fluids, Wertheim's first-order thermodynamic perturbation theory[18] is applied to represent the equation of state in the bulk limit. There exists inconvenient numerical implementation of KR theory;[13] that is, it requires the cavity correlation function of inhomogeneous hard-sphere fluid. The theory proposed by Yu and Wu[19] overcomes this shortcoming, using a radical distribution function represented by the weighted densities from the fundamental measure theory (FMT).[20,21] Their theory gives fairly accurate density profiles and surface excess of confined HSC mixtures,[19] and the intra- and intermolecular radical distribution functions of bulk chain fluids.[22,23] By including the dispersion interaction via mean-field approximation, their theory has been successfully extended to study the structures, adsorptions, wetting, layering, and capillary phase transitions of inhomogeneous polymer melts.[24−26] However, as we have pointed out for atomic fluid, the mean-field approximation is a poor theory for the Helmholtz energy functional due to dispersion interaction.[27−29]

In this paper, the DFT of Yu and Wu[19] is extended to polymeric fluids with dispersion force by introducing a new radial distribution function of polymer monomers in terms of the weighted densities from the FMT and making a functional Taylor expansion proposed by Rosenfeld.[30] The polymer melt is represented by a freely jointed hard-core multi-Yukawa chain fluid which has proven to be a good approximation for alkanes.[31] The bulk direct correlation function from the first-order mean spherical approximation (FMSA)[32] is chosen for the implementation of the excess Helmholtz energy functional due to

* To whom correspondence should be addressed. E-mail: yangxyu@mail.tsinghua.edu.cn.

10.1021/jp060986k CCC: $33.50
Published on Web 07/06/2006

dispersion force. It has been applied to describe the structures, adsorptions, and capillary phase transitions of the hard-core multi-Yukawa chain fluids in slitlike pores. Compared with previous theories[33,34] for confined polymeric fluids, the method reported here has the advantages of simplicity, numerical efficiency, and good accuracy. In the following section, we present the DFT for the hard-core multi-Yukawa chain fluid. We present and discuss the numerical results for the density profiles, bond orientation correlations, adsorption isotherms, and capillary phase transitions in section III, and we end with some conclusions in section IV.

II. Model and Theory

A. Molecular Model. We study the structure and equilibrium phase transition of an inhomogeneous chain fluid which incorporates the relevant features of polymeric materials: excluded volume of segments, chain connectivity, and attractive and repulsive interactions between monomers. The chains are modeled as a pearl necklace of freely jointed hard-core multi-Yukawa spheres with diameter σ. The bonding potential $V_b(\mathbf{R})$ is given by

$$\exp[-V_b(\mathbf{R})/kT] = \prod_{i=1}^{M-1} \frac{\delta(|r_{i+1} - r_j| - \sigma)}{4\pi\sigma^2} \tag{1}$$

where $\mathbf{R} = \{\mathbf{r}_1,\mathbf{r}_2,...,\mathbf{r}_M\}$ is a set of coordinates describing the position of M segments on each chain, $\delta(r)$ is the Dirac delta function, k is the Boltzmann constant, and T is the absolute temperature. The monomeric units interact via a Yukawa potential with multiple tails. This segment−segment interaction $u^Y(r)$ is represented as

$$u^Y(r) = \begin{cases} \infty & r < \sigma \\ -\sum_{i=1}^{m} \dfrac{\epsilon_i \exp[-\lambda_i(r-\sigma)/\sigma]}{r/\sigma} & r \geq \sigma \end{cases} \tag{2}$$

where σ is the diameter of segments, r is the center-to-center distance between two interacting segments, m is the number of tails, ϵ_i and λ_i represent, respectively, the potential energy at contact and the screening length of Yukawa tail i.

We model the pore as a slit formed by two parallel attractive walls separated by a distance of $H + \sigma$. Each monomer on the chains interacts with the walls via a Yukawa-type potential given by

$$\upsilon_i^{ext}(z) = \begin{cases} W(z) + W(H - z) & 0 \leq z \leq H \\ \infty & \text{otherwise} \end{cases} \tag{3}$$

with

$$W(z) = -\epsilon_W \exp(-\lambda_W z/\sigma) \tag{4}$$

where z is the normal distance from the left wall, λ_W and ϵ_W are, respectively, the interaction range and strength parameters between the monomers and the wall. Increasing ϵ_W, the wall attracts the fluid and eventually the fluid will wet the wall.

B. Density Functional Theory. For the model system considered above, the density functional theory can be obtained by extending our previous theory[19] to the hard-sphere chain (HSC) fluid. Generally, the grand potential functional Ω is related to the Helmholtz energy functional F via a Legendre transform

$$\Omega = F[\rho_M(\mathbf{R})] + \int d\mathbf{R}\rho_M(\mathbf{R})[V_M^{ext}(\mathbf{R}) - \mu_M] \tag{5}$$

where $d\mathbf{R} = d\mathbf{r}_1\, d\mathbf{r}_2 \ldots d\mathbf{r}_M$ represents a set of differential volumes for the polymer chain of M segments, μ_M is the polymer chemical potential, and $V_M^{ext}(\mathbf{R})$ denotes the total external potential on the chain. The total potential on each chain molecule is equal to the sum of the potential energy on its individual segments, that is, $V_M^{ext}(\mathbf{R}) = \sum_{i=1}^{M} \upsilon_i^{ext}(\mathbf{r}_i)$.

The Helmholtz energy functional F can be formally expressed as an ideal-gas contribution F_{id} plus an excess term F_{ex} that accounts for intra- and intermolecular interactions other than the bonding potential

$$F = F_{id} + F_{ex} \tag{6}$$

where F_{id} is the ideal-gas contribution given exactly by

$$F_{id} = kT\int d\mathbf{R}\rho_M(\mathbf{R})[\ln \rho_M(\mathbf{R}) - 1] + \int d\mathbf{R}\rho_M(\mathbf{R})\, V_b(\mathbf{R}) \tag{7}$$

To derive the excess Helmholtz energy functional due to both intra- and intermolecular interactions, we decompose F_{ex} into three parts

$$F_{ex} = F_{hs}[\rho(\mathbf{r})] + F_{ch}[\rho(\mathbf{r})] + F_{dis}[\rho(\mathbf{r})] \tag{8}$$

where $\rho(\mathbf{r})$ represents the total segment density profile. The subscripts hs, ch, and dis denote, respectively, contributions to the excess Helmholtz energy functional due to the hard-core repulsion, chain formation, and long-ranged dispersive forces. In writing eq 8, we assume that the excess Helmholtz energy functional can be effectively accounted for by using only segment densities. The total segment density $\rho(\mathbf{r})$ is given by a sum of that for individual segments

$$\rho(\mathbf{r}) = \sum_{i=1}^{M} \rho_{si}(\mathbf{r}) = \sum_{i=1}^{M} \int d\mathbf{R}\, \delta(\mathbf{r} - \mathbf{r}_i)\, \rho(\mathbf{R}) \tag{9}$$

where $\rho_{si}(\mathbf{r})$ stands for the local density of segment i on the chain.

The excess Helmholtz energy functional due to the hard-core repulsion is well described by the modified fundamental measure theory (MFMT),[21] that is,

$$F_{hs} = kT\int d\mathbf{r}\{\Phi^{hs(S)}[n_\alpha(\mathbf{r})] + \Phi^{hs(V)}[n_\alpha(\mathbf{r})]\} \tag{10}$$

where the superscripts (S) and (V) represent the contributions from scalar- and vector-weighted densities, respectively. The scalar Helmholtz energy density is given by

$$\Phi^{hs(S)}[n_\alpha(\mathbf{r})] = -n_0 \ln(1 - n_3) + \frac{n_1 n_2}{1 - n_3} + \frac{{n_2}^3 \ln(1 - n_3)}{36\pi {n_3}^2} + \frac{{n_2}^3}{36\pi n_3 (1 - n_3)^2} \tag{11}$$

and the vector part is expressed by

$$\Phi^{hs(V)}[n_\alpha(\mathbf{r})] = -\frac{\mathbf{n}_{V1}\cdot\mathbf{n}_{V2}}{1 - n_3} - \frac{n_2 \mathbf{n}_{V2}\cdot\mathbf{n}_{V2} \ln(1 - n_3)}{12\pi {n_3}^2} - \frac{n_2 \mathbf{n}_{V2}\cdot\mathbf{n}_{V2}}{12\pi n_3 (1 - n_3)^2} \tag{12}$$

In the above equations, the weighted densities $n_\alpha(\mathbf{r})$ are defined as

$$n_\alpha(\mathbf{r}) = \int d\mathbf{r}'\, \rho(\mathbf{r}')\, w^{(\alpha)}(\mathbf{r}' - \mathbf{r}) \tag{13}$$

where $\alpha = 0, 1, 2, 3, V1$, and $V2$ denote the index of six weight functions $w^{(\alpha)}(\mathbf{r})$. The six weight functions are independent of the density profiles, which are given by

$$w^{(2)}(r) = \pi\sigma^2 w^{(0)}(r) = 2\pi\sigma w^{(1)}(r) = \delta(\sigma/2 - r) \tag{14}$$

$$w^{(3)}(r) = \Theta(\sigma/2 - r) \tag{15}$$

$$\mathbf{w}^{(V2)}(\mathbf{r}) = 2\pi\sigma \mathbf{w}^{(V1)}(\mathbf{r}) = (\mathbf{r}/r)\delta(\sigma/2 - r) \tag{16}$$

where $\Theta(r)$ is the Heaviside step function.

According to our previous work, the Helmholtz energy functional due to chain formation under inhomogeneous conditions can be obtained by extending the first-order thermodynamic perturbation theory[19]

$$\beta F_{ch} = \frac{1 - M}{M} \int d\mathbf{r} n_0 \zeta \ln g(\sigma, n_\alpha) \tag{17}$$

where $\beta = 1/kT$, $\zeta = 1 - \mathbf{n}_{V2}\cdot\mathbf{n}_{V2}/n_2^2$ is an inhomogeneity factor, and $g(\sigma,n_\alpha)$ is the radial distribution function of hard-core multi-Yukawa monomers. To obtain a more accurate radial distribution function $g(\sigma,n_\alpha)$ for multi-Yukawa monomers, the following SEXP approximation is employed:

$$g(\sigma, n_\alpha) = g^{hs}(\sigma, n_\alpha) \exp[g^{(1)}(\sigma, n_\alpha)] \tag{18}$$

where $g^{hs}(\sigma,n_\alpha)$ is the radial distribution function of hard-sphere fluid and $g^{(1)}(\sigma,n_\alpha)$ is the first-order approximation of the radial distribution function of multi-Yukawa spheres. $g^{hs}(\sigma,n_\alpha)$ has been obtained before and is given by[19]

$$g^{hs}(\sigma, n_\alpha) = \frac{1}{(1 - n_3)} + \frac{n_2\sigma\zeta}{4(1 - n_3)^2} + \frac{n_2^2\sigma^2\zeta}{72(1 - n_3)^3} \tag{19}$$

In this work, the expression for $g^{(1)}(\sigma,n_\alpha)$ is modified from the solution of the FMSA for hard-core multi-Yukawa mixtures. From Tang's work,[35] we can obtain the following expression for $g^{(1)}(\sigma,n_\alpha)$ at bulk limit:

$$g^{(1)}(\sigma) = \sum_{i=1}^{m} \beta\epsilon_i [B(\lambda_i)]^2 \tag{20}$$

where

$$B(\lambda_i) = 1 + \frac{2\pi P_n(\lambda_i)\rho}{[\Delta - 2\pi P_n(\lambda_i)\rho]} \tag{21}$$

$$P_n(\lambda_i) = \varphi_2(\lambda_i)P_0 + \varphi_1(\lambda_i)P_1 \tag{22}$$

$$P_0 = 1 + 3\xi_3/\Delta \tag{23}$$

$$P_1 = \sigma + 3\xi_2\sigma^2/(2\Delta) \tag{24}$$

$$\varphi_1(\lambda_i) = \frac{\sigma^2(1 - \lambda_i - e^{-\lambda_i})}{\lambda_i^2} \tag{25}$$

$$\varphi_2(\lambda_i) = \frac{\sigma^3(1 - \lambda_i + \lambda_i^2/2 - e^{-\lambda_i})}{\lambda_i^3} \tag{26}$$

with $\xi_n = (\pi/6)\sum\rho_k\sigma_k^n$ (superscript $n = 0, 1, 2, 3$) and $\Delta = 1 - \xi_3$. It should be mentioned that another expression for $g^{(1)}(\sigma)$ derived by Tang et al.[36] results in the same values of $g^{(1)}(\sigma)$ as the above equations at bulk limit. We prefer eqs 20−26 because they are easy to be extended to inhomogeneous fluid in terms of the FMT. Using the rule proposed previously,[7] we obtain the following expression for $g^{(1)}(\sigma,n_\alpha)$

$$g^{(1)}(\sigma, n_\alpha) = \sum_{i=1}^{m} \beta\epsilon_i [B(\lambda_i, n_\alpha)]^2 \tag{27}$$

$$B(\lambda_i, n_\alpha) = 1 + \frac{2\pi n_0 \zeta P_n(\lambda_i, n_\alpha)}{[1 - n_3 - 2\pi n_0 \zeta P_n(\lambda_i, n_\alpha)]} \tag{28}$$

$$P_n(\lambda_i, n_\alpha) = \varphi_2(\lambda_i)P_0(n_\alpha) + \varphi_1(\lambda_i)P_1(n_\alpha) \tag{29}$$

$$P_0(n_\alpha) = 1 + 3n_3/(1 - n_3) \tag{30}$$

$$P_1(n_\alpha) = \sigma + n_2\zeta\sigma^2/[4(1 - n_3)] \tag{31}$$

Finally, the dispersion part of the excess Helmholtz energy functional F_{dis} is approximated by a functional Taylor expansion

$$F_{dis} = -\frac{kT}{2} \int\int d\mathbf{r}\, d\mathbf{r}' \Delta C_{MY}^{(2)b}(|\mathbf{r}' - \mathbf{r}|)\, \rho(\mathbf{r})\, \rho(\mathbf{r}') \tag{32}$$

where $\Delta C_{MY}^{(2)b}(r) = C_{MY}^{(2)b}(r) - C_{hs}^{(2)b}(r)$ and $C_{MY}^{(2)b}(r)$ and $C_{hs}^{(2)b}(r)$ are the bulk second-order direct correlation functions for hard-core multi-Yukawa fluid and hard-sphere fluid, respectively. In this work, $\Delta C_{MY}^{(2)b}(r)$ is obtained from the FMSA solution for the corresponding hard-core multi-Yukawa fluid in the bulk case.[29,36]

Minimization of the grand potential with respect to the density profile $\rho_M(\mathbf{R})$ yields the following Euler−Lagrange equation:

$$\rho_M(\mathbf{R}) = \exp[\beta\mu_M - \beta V_b(\mathbf{R}) - \beta V_M^{ext}(\mathbf{R}) - \beta\Lambda(\mathbf{R})] \tag{33}$$

where $\Lambda(\mathbf{R}) = \delta F_{ex}/\delta\rho_M(\mathbf{R})$. Because the excess Helmholtz energy functional used in this work depends only on the segment density profile $\rho(\mathbf{r})$, $\Lambda(\mathbf{R})$ can be simplified to

$$\Lambda(\mathbf{R}) = \frac{\delta F_{ex}}{\delta\rho_M(\mathbf{R})} = \sum_{i=1}^{M} \frac{\delta F_{ex}}{\delta\rho(\mathbf{r}_i)} \tag{34}$$

Substituting eq 34 into eq 33 yields

$$\rho_M(\mathbf{R}) = \exp[\beta\mu_M - \beta V_b(\mathbf{R}) - \beta\sum_{i=1}^{M} \psi_i(\mathbf{r}_i)] \tag{35}$$

where $\psi_i(\mathbf{r}_i)$ is related to the excess Helmholtz energy functional F_{ex} and the external potential $v_i^{ext}(\mathbf{r}_i)$ by

$$\psi_i(\mathbf{r}_i) = \delta F_{ex}/\delta\rho(\mathbf{r}_i) + v_i^{ext}(\mathbf{r}_i) \tag{36}$$

Equation 35 indicates that as in a typical self-consistent-field theory, the segment density is determined by the chain connectivity and an effective external potential $\psi_i(\mathbf{r}_i)$. Because eq 35 involves only the total segment density, the self-consistent field is identical for all segments.

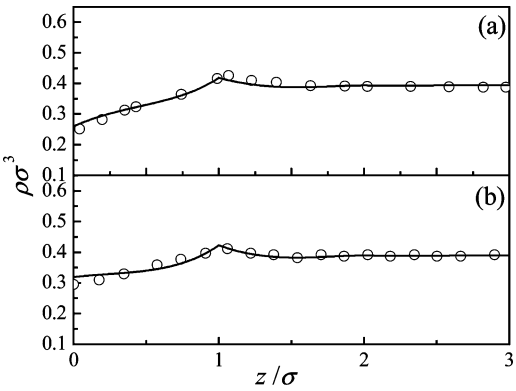

Figure 1. Reduced density profiles of one-Yukawa 10-mers ($\lambda_1 = 2.5$) in a slitlike pore ($H = 10\sigma$, $\lambda_W = 2.5$) at a reduced temperature of $T^* = 5.0$ and an average packing fraction of $\eta_{av} = 0.2$ for the wall energy parameters: (a) $\epsilon_W = 0$; (b) $\epsilon_W/\epsilon_1 = 1.0$. The symbols and solid curves represent the results from the CMC simulations of Goel et al.[33] and the present DFT, respectively.

From eqs 7 and 35, we can obtain the total segment density profile

$$\rho(\mathbf{r}) = \int d\mathbf{R} \sum_{i=1}^{M} \delta(\mathbf{r} - \mathbf{r}_i) \exp[\beta\mu_M - \beta V_b(\mathbf{R}) - \beta \sum_{i=1}^{M} \psi_i(\mathbf{r}_i)] \quad (37)$$

For a polymer confined in a slitlike pore, the segment density distribution varies only in the z-direction. In this case, the multidimensional integral in eq 37 can be simply factored as

$$\rho_{si}(z) = \exp[\beta\mu_M - \beta\psi_i(z)] G_L^i(z)\, G_R^i(z) \quad (38)$$

where $G_L^i(z)$ is determined from the recurrence relation

$$G_L^i(z) = \int dz' \exp[-\beta\psi_i(z')] \frac{\theta(\sigma - |z' - z|)}{2\sigma} G_L^{i-1}(z') \quad (39)$$

for $i = 2, \ldots, M$ with $G_L^1(z) = 1$. Because the external potential is the same for all the monomers on the chain, we have the symmetric relation

$$G_R^{M-i+1}(z) = G_L^i(z) \quad (40)$$

The chemical potential for solving the segment density profiles is obtained from eq 38 by switching off the external potential $V_M^{ext}(\mathbf{R})$. The segment density profiles are solved using the Picard-type iteration method through eqs 38−40. The iteration repeats until the relative percentage change is smaller than 0.01% at all points. The numerical integrations are performed using the trapezoidal rule with the step size $\Delta z = 0.005\sigma$.

III. Results and Discussion

A. Density Profiles. As a test of our DFT, we compare the density profiles predicted from the present DFT with that from the canonical ensemble Monte Carlo (CMC) simulations. For direct comparison, the bulk density in the DFT calculations is adjusted such that the two approaches yield the same average segment density in the pore. Figures 1−4 present the theoretical predictions for hard-core one-Yukawa 5-mers, 10-mers, and 20-mers, along with the CMC simulation results[33] under various conditions. For each set of density and temperature, two wall energy parameters, $\epsilon_W/\epsilon_1 = 0$ and 1.0, are considered. Here, the average packing fraction η_{av} is defined as $\eta_{av} = \pi\rho_{av}\sigma^3/6$,

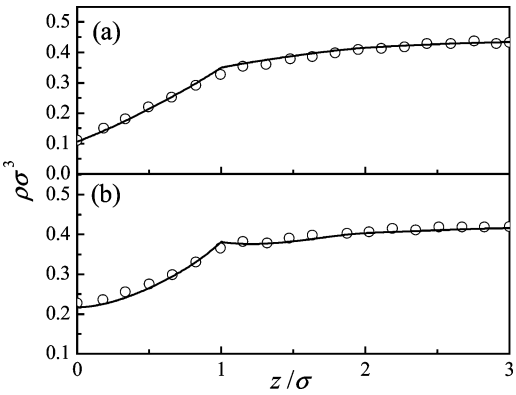

Figure 2. Same as Figure 1 but with $T^* = 2.0$.

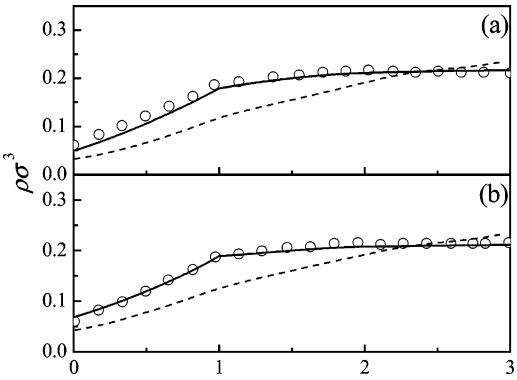

Figure 3. Reduced density profiles of one-Yukawa 20-mers ($\lambda_1 = 2.5$) in a slitlike pore ($H = 10\sigma$, $\lambda_W = 2.5$) at a reduced temperature of $T^* = 5.0$ and an average packing fraction of $\eta_{av} = 0.1$ for the wall energy parameters: (a) $\epsilon_W = 0$; (b) $\epsilon_W/\epsilon_1 = 1.0$. The symbols, dashed, and solid curves represent the results from the CMC simulations, theory of Goel et al.,[33] and the present DFT, respectively.

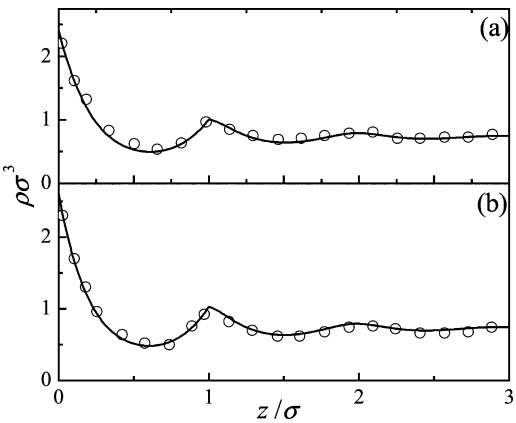

Figure 4. Reduced density profiles of one-Yukawa 5-mers ($\lambda_1 = 2.5$) in a slitlike pore ($H = 10\sigma$, $\lambda_W = 2.5$) at a reduced temperature of $T^* = 5.0$ and an average packing fraction of $\eta_{av} = 0.4$ for the wall energy parameters: (a) $\epsilon_W = 0$; (b) $\epsilon_W/\epsilon_1 = 1.0$. The symbols and solid curves represent the results from the CMC simulations of Goel et al.[33] and the present DFT, respectively.

where ρ_{av} is the average number density of segment given by

$$\rho_{av} = \int_0^H \rho(z)\, dz/H \quad (41)$$

and the reduced temperature is defined as $T^* = kT/\epsilon_1$. From Figures 1−4, one can see that the behavior of the density profiles of hard-core one-Yukawa chains confined between hard walls ($\epsilon_W = 0$) is similar to that of the hard-sphere chain fluid. The density profiles are governed by the competition between the

configurational and packing entropic effects. The depletion of density profiles near the wall is shown at low densities, while the opposite trend is found at high densities. In the case of attractive walls ($\epsilon_W/\epsilon_1 = 1.0$), there is a net enhancement of segment density near the surface compared to hard walls at the same reduced temperature. The present DFT is in excellent agreement with the simulation data under all conditions. In particular, the density at contact predicted from the present DFT is very close to the simulation value.

Figures 1 and 2 depict the density profiles of one-Yukawa 10-mers in the slitlike pores at reduced temperatures of $T^* = 5.0$ and 2.0, respectively. At lower reduced temperature ($T^* = 2.0$), the fluid−fluid attraction is stronger and the tendency toward depletion of the region near the wall is more pronounced. In addition, Figures 1−4 show that all the densities near the surfaces for one-Yukawa chains are lower than those for the hard-sphere chain fluids at the same chain length, density, and wall potential parameters. This phenomenon is similar to that we found from the hard-core repulsive and attractive Yukawa fluids before.[28] All of these indicate that the intermolecular attraction and chain formation cause a depletion of chain segments near a wall, while the intermolecular repulsion and packing effect lead to an enhancement of chain segments near the wall.

The comparisons of the predictions from the present DFT with that from the theory of Goel et al.[33] for one-Yukawa 20-mers are shown in Figure 3. The present DFT gives very accurate density profiles near the wall, while the theory of Goel et al.[33] underestimates the layering of the chain at the surface under these conditions. This deficiency in their theory can be improved by a proper choice of bridge function. An important difference between two theories is that the intramolecular interaction $V_b(\mathbf{R})$ in the inhomogeneous fluid is obtained by carrying out Monte Carlo simulation of a single chain in the theory of Goel et al.,[33] whereas intramolecular correlations and segment density profiles are obtained in a self-consistent manner in the present theory. The advantage of the present DFT is that it uses the analytical direct correlation function from the FMSA and avoids solving the nonlinear PRISM integral equation numerically in the calculation. This makes the present DFT easier to implement.

B. Chain Conformations. The present DFT can provide the local information about the orientation of each bond along the chain. The orientation of each chain segment in the inhomogeneous condition is generally presented by the bond orientation correlation function $s(z)$ defined as

$$s(z) = [3\langle \cos \omega \rangle - 1]/2 \tag{42}$$

where s is the bond anisotropy factor, ω is the angle between the bond (vector joining the centers of adjacent segments i and $i + 1$ on a chain) and the z axis (normal to the wall), z is the coordinate of the bond middle point, and $\langle \cdots \rangle$ stands for the average over all bonds and configurations. For the model considered in this work, it is easy to see that $\sigma \cos \omega = z_{i+1} - z_i$. To evaluate this quantity, we need a set of intramolecular distribution functions $\rho_{i,i+1}(z,z')$ defined by

$$\rho_{i,i+1}(\mathbf{r},\mathbf{r}') = \int d\mathbf{R} \delta(\mathbf{r} - \mathbf{r}_i)\, \delta(\mathbf{r}' - \mathbf{r}_{i+1})\, \rho_M(\mathbf{R}) \tag{43}$$

From eq 43 and the Euler−Lagrange equation (eq 35), we can obtain the factorization expression of $\rho_{i,i+1}(z,z')$

$$\rho_{i,i+1}(z,z') = \exp[\beta\mu_M - \beta\psi_i(z) - \beta\psi_i(z')] \frac{\theta(\sigma - |z - z'|)}{2\sigma} G_L^i(z)\, G_R^{i+1}(z') \tag{44}$$

Then, the bond orientation correlation function is easily evaluated from

$$\langle \cos \omega \rangle = \frac{1}{M-1} \sum_{i=1}^{M-1} \frac{\int_{-1}^{1} dy \rho_{i,i+1}\left(z - \frac{\sigma}{2}y, z + \frac{\sigma}{2}y\right) y^2}{\int_{-1}^{1} dy \rho_{i,i+1}\left(z - \frac{\sigma}{2}y, z + \frac{\sigma}{2}y\right)} \tag{45}$$

where $y = \cos \omega$. From the definition of the bond orientation correlation function, we know that $s(z) = -0.5$ denotes that bonds are parallel to the solid walls, $s(z) = 0$ corresponds to randomly oriented bonds, and $s(z) = 1.0$ denotes that bonds are normal to the solid walls.

In Figure 5, we compare the bond orientation correlation functions predicted from the present DFT with that from the CMC simulations for hard-core one-Yukawa 10-mers in a hard slitlike pore ($H = 10\sigma$, $\epsilon_W = 0$) at reduced temperature $T^* = \infty$ and average packing fraction $\eta_{av} = 0.1$ and 0.4. In this limit of reduced temperature, the hard-core one-Yukawa chain fluid is reduced to HSC fluid. The agreements between the present DFT predictions and the CMC simulation data are very good. Figure 5 shows that the bond anisotropy persists only half or one segment diameter at low density and persists over three or four segment diameters at high density, just like the density inhomogeneities in the pore.

The effects of fluid−fluid and fluid−wall attractions on the bond orientations in a slitlike pore ($H = 10\sigma$, $\lambda_W = 1.8$) for two-Yukawa 20-mers ($\lambda_1 = 2.8647$, $\lambda_2 = 13.5485$, $\epsilon_2/\epsilon_1 = -1.4466$) are presented in Figures 6 and 7 for bulk packing fraction $\eta_b = 0.2$ and 0.35, respectively. In this case, the two-Yukawa monomers mimic the Lennard-Jones potential, which is repulsive near the contact distance and becomes attractive at long enough distance. Nevertheless, the attractive dispersion force is dominant in this case. Figures 6 and 7 suggest that the chain segments are aligned parallel to the solid surface in its vicinity. The bond anisotropy of the two-Yukawa 20-mers persists for a short distance at low density, and the strong oscillations of the bond orientation correlation function are observed at high density. When the intermolecular attraction between chain segments appears, the oscillations of the bond orientation correlation function become less pronounced. On the other hand, the introduction of the fluid−wall attraction enhances the oscillations. The preferential normal to the wall alignment (peak to profiles as shown in Figure 7) is closely related to the segment layering. It reflects the necessity for bonds having their middlepoints in this region to connect segments in the first and second layer, and therefore to have an orientation more or less normal to the solid surface.

C. Adsorption and Capillary Phase Equilibrium. We now apply the present DFT to the multi-Yukawa chain fluids with a special attention given to the effect of fluid−fluid and fluid−wall attractions on adsorption and capillary phase transition in slitlike pores. Figure 8 compares the adsorption isotherms of hard-sphere, one-Yukawa ($\lambda_1 = 1.8$) and two-Yukawa ($\lambda_1 = 1.8$, $\lambda_2 = 4.0$, $\epsilon_2/\epsilon_1 = -1.0$) 20-mers confined in a hard slitlike pore at a reduced temperature of $T^* = 3.5$. Here, for the one-Yukawa 20-mers, the monomers interact with each other by an attractive Yukawa potential, while, for the two-Yukawa 20-mers, the potential between the monomers is zero at contact and

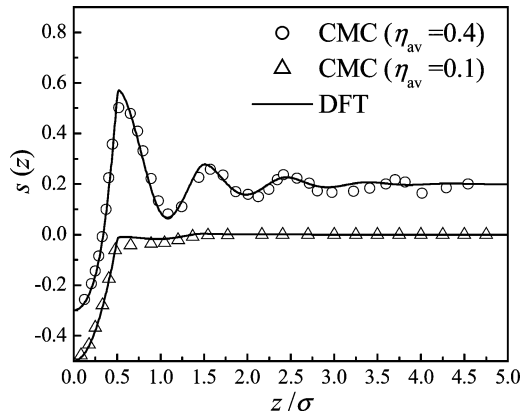

Figure 5. Comparison of bond orientation correlation function predicted from the present DFT with those from CMC simulations for one-Yukawa 10-mers in a slitlike pore ($H = 10\sigma$, $\epsilon_W = 0$) at a reduced temperature of $T^* = \infty$ and an average packing fraction of $\eta_{av} = 0.1$ and 0.4. The symbols and solid curves represent the results from the CMC simulations of Goel et al.[33] and the present DFT, respectively.

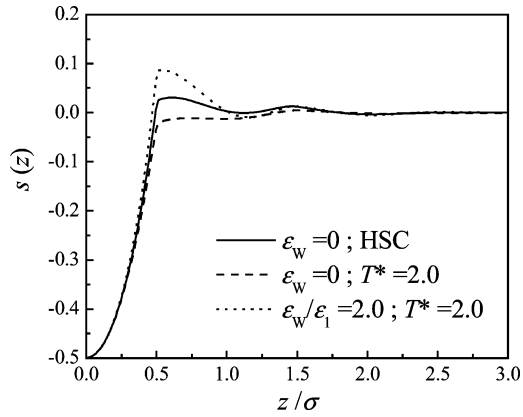

Figure 6. Bond orientation correlation function predicted from the present DFT for two-Yukawa 20-mers ($\lambda_1 = 2.8647$, $\lambda_2 = 13.5485$, $\epsilon_2/\epsilon_1 = -1.4466$) confined in a slitlike pore ($H = 10\sigma$, $\lambda_W = 1.8$) at a bulk packing fraction of $\eta_b = 0.2$ and various values of temperatures and wall energy parameters.

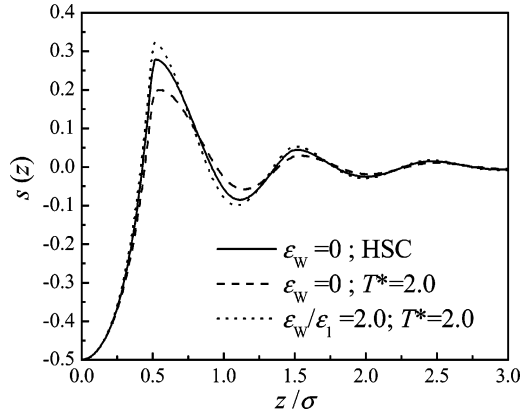

Figure 7. Same as Figure 6 but with $\eta_b = 0.35$.

becomes attractive at long distance. Overall, the attractive force between the two-Yukawa monomers is smaller than that between one-Yukawa monomers. The excess adsorption is defined as

$$\Gamma^{ex} = \int_0^H [\rho(z) - \rho_b]\, dz \qquad (46)$$

From Figure 8, one can see that, for polymeric fluids confined in a hard slitlike pore ($H = 10\sigma$, $\epsilon_W = 0$), the excess adsorption Γ^{ex} is negative at low density and becomes positive at high

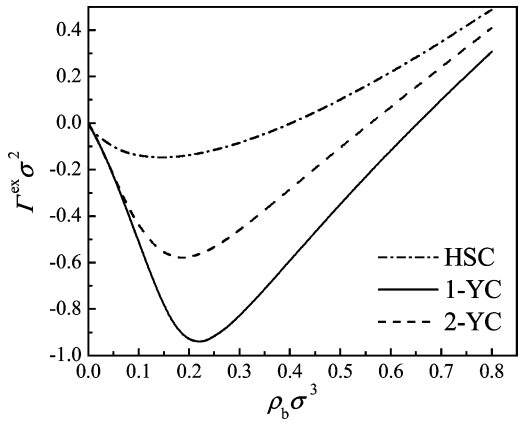

Figure 8. Adsorption isotherms predicted from the present DFT for hard-sphere, one-Yukawa ($\lambda_1 = 1.8$) and two-Yukawa ($\lambda_1 = 1.8$, $\lambda_2 = 4.0$, $\epsilon_2/\epsilon_1 = -1.0$) 20-mers in a slitlike pore ($\epsilon_W = 0$, $H = 10\sigma$) at a reduced temperature of $T^* = 3.5$. Dash−dotted, dashed, and solid curves represent the results for hard-sphere, one-Yukawa and two-Yukawa chains, respectively.

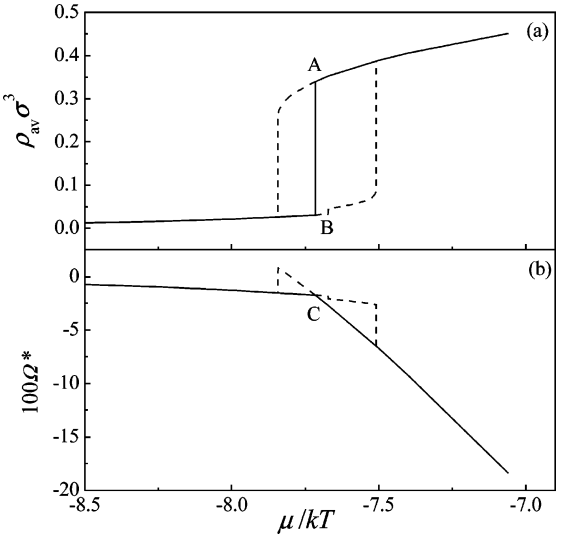

Figure 9. The predicted results of (a) the average density and (b) reduced grand potential as a function of the chemical potential for two-Yukawa 4-mers ($\lambda_1 = 2.673$; $\lambda_2 = 4.408$; $\epsilon_2/\epsilon_1 = -3.955/4.755$) in a hard slitlike pore ($\epsilon_W = 0$, $H = 5\sigma$) at a reduced temperature of $T^* = 0.6$. The solid curves represent the thermodynamically stable states, and the dashed curves denote the metastable states.

enough density. This can be well understood by the competition between chain configurational and packing entropic effects. It is interesting to see that the attraction between chain segments substantially decreases the excess adsorption Γ^{ex} of chain fluids in the hard slitlike pore. Because the temperature in this figure is higher than the critical points of both one- and two-Yukawa chain fluids, no capillary condensation is observed.

Figure 9 depicts the adsorption/desorption isotherms and reduced grand potential of two-Yukawa 4-mers ($\lambda_1 = 2.673$, $\lambda_2 = 4.408$, $\epsilon_2/\epsilon_1 = 3.955/4.755$) confined in a hard slitlike pore ($H = 5\sigma$, $\epsilon_W = 0$) at a reduced temperature of $T^* = 0.6$. Here, the reduced grand potential is defined as $\Omega^* = \Omega\sigma^2/AkT$, where A is the surface area. The capillary condensation phenomenon takes place and can be clearly observed in the figure. The solid vertical line connecting points A and B in Figure 9a represents the equilibrium capillary phase transition, corresponding to the crossover point C in Figure 9b. This indicates that, at equilibrium phase transition in the pore, both the chemical potential and grand potential in the liquidlike phase are equal to that in the

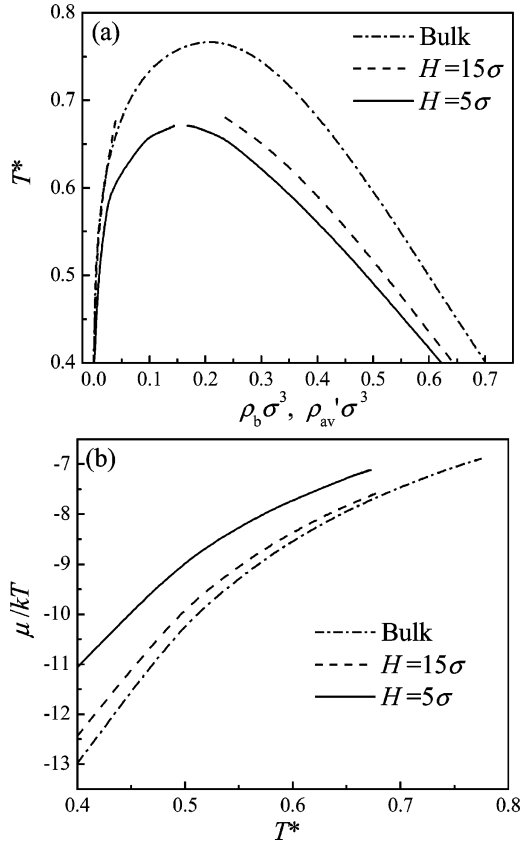

Figure 10. Phase diagram predicted from the present DFT for the two-Yukawa 4-mers ($\lambda_1 = 2.673$; $\lambda_2 = 4.408$; $\epsilon_2/\epsilon_1 = -3.955/4.755$) confined in the hard slitlike pores ($\epsilon_W = 0$): (a) $T^*-\rho'_{av}\sigma^3$ projections; (b) $\mu/kT-T^*$ projections. The solid, dashed, and dash−dotted curves represent the results for the pore width $H = 5\sigma$, the pore width $H = 15\sigma$, and the bulk case, respectively.

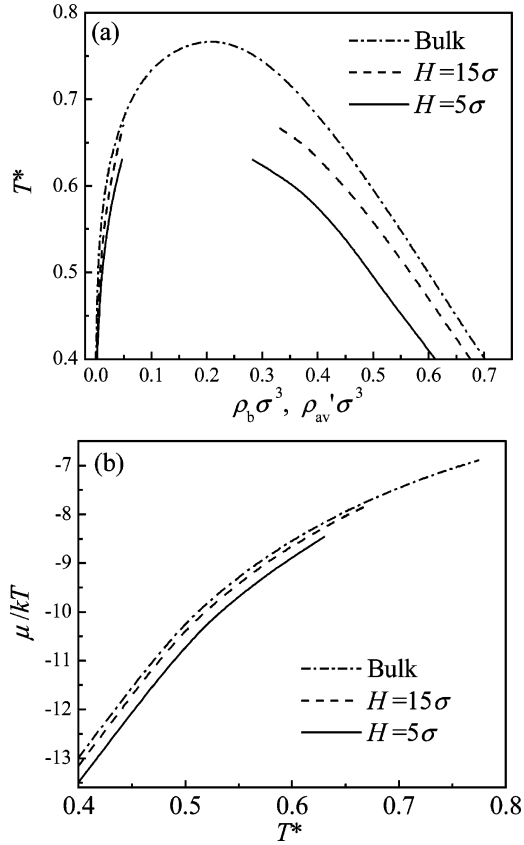

Figure 11. Same as Figure 10 but for the wall energy parameter $\epsilon_W/\epsilon_1 = 1.0$.

gaslike phase. For the polymeric fluid confined in a hard slitlike pore, no layering transition can be found.

From the adsorption/desorption isotherms and grand potential presented in Figure 9, we can determine the coexistence density for the equilibrium capillary phase transition. Figures 10 and 11 depict the phase diagrams of confined and bulk two-Yukawa 4-mers ($\lambda_1 = 2.673$, $\lambda_2 = 4.408$, $\epsilon_2/\epsilon_1 = 3.955/4.755$) at wall parameters of $\lambda_W = 1.8$ and $\epsilon_W/\epsilon_1 = 0$ and 1.0. Here, the average density over the entire pore is calculated from $\rho'_{av} = \rho_{av}H/(H + \sigma)$. In both hard and attractive pores, the effect of the pore width on the $T^*-\rho'_{av}\sigma^3$ diagram is similar; that is, the confinement lowers the critical temperature and the lowering is larger for narrower pores. The average liquidlike density ρ'_{av} of the confined chain fluid is always lower than that in the bulk phase. On the other hand, the density of the dilute vaporlike phase is less affected by the confinement: it may be lower or higher than the bulk vapor density (see Figure 10a). However, there is a qualitative difference between hard and attractive pores on $\mu/kT-T^*$ diagrams. Figure 10b shows that the equilibrium capillary phase transition of the chain fluid in the hard slitlike pore occurs at a higher chemical potential than in bulk condition. As the attraction of the pore wall is increased, the chemical potential for equilibrium capillary phase transition of the confined chain fluid becomes lower than that for bulk vapor−liquid equilibrium, as shown in Figure 11b. Because we focus on the equilibrium capillary phase transition, there is no layering transition at the wall parameters considered here. If the wall energy parameter ϵ_W is large enough, the layering transition of a multi-Yukawa chain fluid in a pore will occur.[24]

IV. Conclusions

A density functional theory is presented to investigate the density profiles, chain conformations, and equilibrium capillary phase transition of freely jointed hard-core multi-Yukawa chain fluids confined in slitlike pores, including the effects of fluid−fluid and fluid−wall attractions. The excess Helmholtz energy functional is constructed by using the modified fundamental measure theory of Yu and Wu for hard-core contribution, the first-order thermodynamic perturbation theory for chain formation, and Rosenfeld's perturbative method for dispersion contribution. The required radial distribution function and bulk second-order direct correlation function for multi-Yukawa monomers are obtained from the analytical solution of the Ornstein−Zernike integral equation with the first-order mean spherical approximation. The obtained theory avoids the numerical solution of the integral equation and is easy to implement. Comparisons of the density profiles predicted from the present density functional theory with that from the canonical Monte Carlo simulations show that the present theory is quite accurate. In contrast, the theory of Goel et al.[33] always underestimates the density profiles of one-Yukawa chain fluids in the slitlike pores. Both theory and simulation indicate that the intermolecular attraction and chain formation cause a depletion of chain segments near a solid surface, while the intermolecular repulsive and packing effect lead to an enhancement of chain segments near a solid surface.

The chain configurations of polymer melts in the slitlike pores are investigated through the bond orientation correlation functions. When the present density functional theory is applied to the calculation of the bond orientation correlation function for hard-sphere chain fluid, an excellent agreement between the predictions and simulation data is achieved. The predictions from the present theory show that the chain segments are aligned

parallel to the solid surface in its vicinity. The bond anisotropy of two-Yukawa 10-mers persists over a short distance (half to one segment diameter), and the strong oscillations of the bond orientation correlation function are observed at high density. The effects of fluid−fluid and fluid−wall attractions on the bond orientation correlation function are similar to that on the corresponding density profiles.

When a polymeric fluid is confined in a slitlike pore, the critical temperature of capillary phase transition is always smaller than that in the bulk case. The coexistence average liquidlike density over the whole pore is always lower than that in the bulk phase, while the density of the dilute vaporlike phase is less affected by the confinement. The chemical potential for the equilibrium capillary phase transition of chain fluids confined in a hard slitlike pore ($\epsilon_W = 0$) is higher than that for the bulk vapor−liquid equilibrium, but if the attraction of the pore wall is strong enough, it becomes lower than that in the bulk case.

Acknowledgment. The financial support of the National Natural Science Foundation of China under Grant No. 20376037 and the National Basic Research Program of China under Grant No. 2003CB615700 is acknowledged.

References and Notes

(1) Israelachvili, J. N. *Intermolecular and Surface Forces*; Academic: London, 1992.
(2) Honnell, K. G.; Hall, C. K. *J. Chem. Phys.* **1991**, *95*, 4481.
(3) Yethiraj, A.; Hall, C. K. *J. Chem. Phys.* **1991**, *95*, 3749.
(4) Scheutjens, J. M. H. M.; Fleer, G. J. *J. Phys. Chem.* **1980**, *84*, 178.
(5) Daoulas, K. C.; Theodorou, D. N.; Harmandaris, V. A.; Karayiannis, N. C.; Mavrantzas, V. G. *Macromolecules* **2005**, *38*, 7134.
(6) Henderson, D. *Fundamentals of Inhomogeneous Fluids*; Dekker: New York, 1992.
(7) Yu, Y.-X.; Wu, J. Z. *J. Chem. Phys.* **2002**, *116*, 7094.
(8) Chandler, D.; McCoy, J. D.; Singer, S. J. *J. Chem. Phys.* **1986**, *85*, 5971.
(9) Chandler, D.; McCoy, J. D.; Singer, S. J. *J. Chem. Phys.* **1986**, *85*, 5977.
(10) McCoy, J. D.; Singer, S. J.; Chandler, D. *J. Chem. Phys.* **1987**, *87*, 4853.
(11) Hooper, J. B.; McCoy, J. D.; Curro, J. G.; van Swol, F. *J. Chem. Phys.* **2000**, *113*, 2021.
(12) Woodward, C. E. *J. Chem. Phys.* **1991**, *94*, 3183.
(13) Kierlik, E.; Rosinberg, M. L. *J. Chem. Phys.* **1993**, *100*, 1716.
(14) Yethiraj, A.; Woodward, C. E. *J. Chem. Phys.* **1995**, *102*, 5499.
(15) Patra, C. N.; Yethiraj, A. *J. Chem. Phys.* **2000**, *112*, 1579.
(16) Ye, Z. C.; Cai, J.; Liu, H. L.; Hu, Y. *J. Chem. Phys.* **2005**, *123*, 194902.
(17) Ye, Z. C.; Cai, J.; Zhang, S. L.; Liu, H. L.; Hu, Y. *Acta Phys. Sin.* **2005**, *54*, 4044.
(18) Wertheim, M. S. *J. Stat. Phys.* **1986**, *42*, 477.
(19) Yu, Y.-X.; Wu, J. Z. *J. Chem. Phys.* **2002**, *117*, 2368.
(20) Rosenfeld, Y. *Phys. Rev. Lett.* **1989**, *63*, 980.
(21) Yu, Y.-X.; Wu, J. Z. *J. Chem. Phys.* **2002**, *117*, 10156.
(22) Yu, Y.-X.; Wu, J. Z. *J. Chem. Phys.* **2003**, *118*, 3835.
(23) Yu, Y.-X.; Wu, J. Z.; You, F.-Q.; Gao, G.-H. *Chin. Phys. Lett.* **2005**, *22*, 246.
(24) Bryk, P.; Bucior, S.; Sokolowski, S.; Zukocinski, G. *J. Phys. Chem. B* **2005**, *109*, 2977.
(25) Bryk, P.; Pizio, O.; Sokolowski, S. *J. Chem. Phys.* **2005**, *122*, 194904.
(26) Bryk, P.; Sokolowski, S. *J. Chem. Phys.* **2004**, *121*, 11314.
(27) Fu, D.; Zhao, Y. *Acta Chim. Sin.* **2005**, *63*, 11.
(28) You, F.-Q.; Yu, Y.-X.; Gao, G.-H. *J. Phys. Chem. B* **2005**, *109*, 3512.
(29) Yu, Y.-X.; You, F.-Q.; Tang, Y. P.; Gao, G.-H.; Li, Y.-G. *J. Phys. Chem. B* **2006**, *110*, 334.
(30) Rosenfeld, Y. *J. Chem. Phys.* **1993**, *98*, 8126.
(31) Fu, D.; Li, Y.-G.; Lu, J.-F. *Acta Chim. Sin.* **2004**, *62*, 1034.
(32) Tang, Y. *J. Chem. Phys.* **2003**, *118*, 4140.
(33) Goel, T.; Patra, C. N.; Ghosh, S. K.; Mukherjee, T. *J. Chem. Phys.* **2004**, *121*, 4865.
(34) Patra, C. N.; Yethiraj, A. *J. Chem. Phys.* **2003**, *118*, 4702.
(35) Tang, Y. *Mol. Phys.* **2002**, *100*, 1033.
(36) Tang, Y.; Lin, Y.-Z.; Li, Y.-G. *J. Chem. Phys.* **2005**, *122*, 184505.